Energy-Cascaded Upconversion in an Organic Dye-Sensitized Core/Shell Fluoride Nanocrystal

Guanying Chen,*,[†,‡] Jossana Damasco,[†] Hailong Qiu,[†,‡] Wei Shao,[†,‡] Tymish Y. Ohulchanskyy,[†] Rashid R. Valiev,[§,‖] Xiang Wu,[⊥] Gang Han,[⊥] Yan Wang,[†] Chunhui Yang,[‡] Hans Ågren,[§] and Paras N. Prasad*,[†,∇]

[†]Institute for Lasers, Photonics, and Biophotonics, University at Buffalo, State University of New York, Buffalo, New York 14260, United States

[‡]School of Chemical Engineering and Technology, Harbin Institute of Technology, Harbin, Heilongjiang 150001, P. R. China

[§]Department of Theoretical Chemistry and Biology, Royal Institute of Technology, S-10691 Stockholm, Sweden

[‖]Tomsk State University, 36 Lenin Avenue, 634050 Tomsk, Russian Federation

[⊥]Department of Biochemistry and Molecular Pharmacology, University of Massachusetts Medical School, Worcester, Massachusetts 01605, United States

[∇]Department of Chemistry, Korea University, Seoul 136-701, Korea

S *Supporting Information*
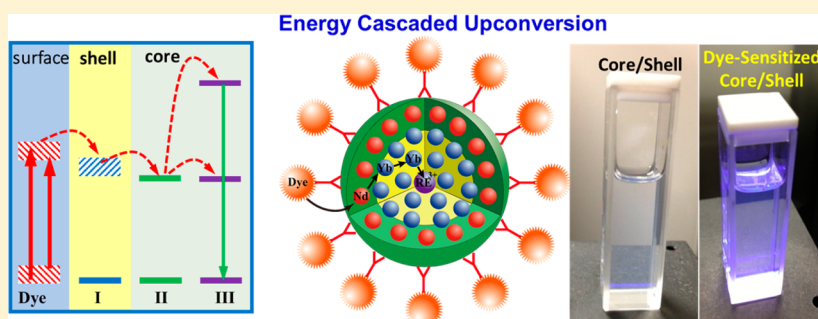
ABSTRACT: Lanthanide-doped upconversion nanoparticles hold promises for bioimaging, solar cells, and volumetric displays. However, their emission brightness and excitation wavelength range are limited by the weak and narrowband absorption of lanthanide ions. Here, we introduce a concept of multistep cascade energy transfer, from broadly infrared-harvesting organic dyes to sensitizer ions in the shell of an epitaxially designed core/shell inorganic nanostructure, with a sequential nonradiative energy transfer to upconverting ion pairs in the core. We show that this concept, when implemented in a core−shell architecture with suppressed surface-related luminescence quenching, yields multiphoton (three-, four-, and five-photon) upconversion quantum efficiency as high as 19% (upconversion energy conversion efficiency of 9.3%, upconversion quantum yield of 4.8%), which is about ∼100 times higher than typically reported efficiency of upconversion at 800 nm in lanthanide-based nanostructures, along with a broad spectral range (over 150 nm) of infrared excitation and a large absorption cross-section of 1.47×10^{-14} cm^2 per single nanoparticle. These features enable unprecedented three-photon upconversion (visible by naked eye as blue light) of an incoherent infrared light excitation with a power density comparable to that of solar irradiation at the Earth surface, having implications for broad applications of these organic−inorganic core/shell nanostructures with energy-cascaded upconversion.

KEYWORDS: Upconversion, Dye-Sensitized, Rare-Earth, Lanthanide, Core/Shell, Nanoparticles

Upconversion nanoparticles (UCNPs) constitute a dilute guest−host system, in which lanthanide ions are doped as a guest in an appropriate dielectric host lattice, such as sodium yttrium fluoride (NaYF$_4$), with a dimension of less than 100 nm.[1] In UCNPs, typically, the doped Yb^{3+} ions (sensitizers) absorb infrared radiation and nonradiatively transfer excitation to the doped activators X^{3+} (X = Er, Ho, Tm) to produce visible or ultraviolet upconversion luminescence (UCL) (Figure 1a). Recent advances have enabled good control over UCNP size, phase, and emission colors.[2−5] An improvement of

the UCL intensity has also been reported through optimizing the concentration and distribution of doped lanthanide sensitizer/activator ions within a single nanoparticle,[6−8] through coating nanoparticles with an inert/active shell to suppress surface-related luminescence quenching[9,10] and by using metallic structures to plasmonically enhance the energy
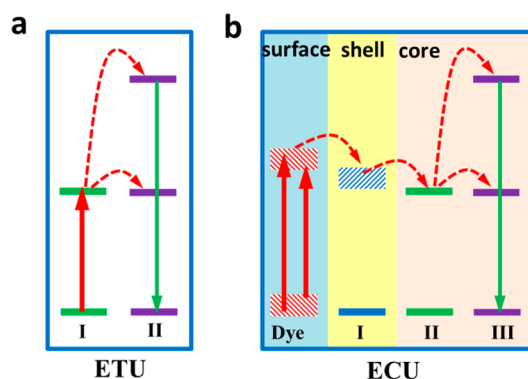
Figure 1. Simplified energy level diagrams depicting the classical and the proposed upconversion processes. (a) Energy transfer upconversion (ETU). An ETU mechanism involves two types of lanthanide ions in which one ion (ion I, sensitizer) successively transfers absorbed energy to a neighboring ion (ion II, activator), exciting ion II to its upper emitting state. (b) Proposed energy-cascaded upconversion (ECU), involving the use of an organic dye, three types of lanthanide ions, and a core−shell design. Note that the nanoparticle surface, the shell, and the core region are highlighted with three distinct colors. The dyes on the nanoparticle surface broadly harvest the excitation energy, which is nonradiatively transferred to the intermediate sensitizers (lanthanide ion I) in the shell, and then across the core/shell interface to the sensitizer (ion II) in the core, and finally to the activator (ion III) also in the core to produce upconversion via the classical ETU mechanism.

transfer rate.[11] However, none of these approaches address the main limitation of UCNPs, namely the narrow and weak absorption associated with the nature of the 4f−4f electronic transitions of lanthanide ions. Specifically, the sensitizer ion Yb^{3+} absorbs light in a narrow spectral window of ∼10 260−10 660 cm^{-1} (∼10 times narrower than that of an organic dye),[12] and with a critically small absorption cross section of ∼10^{-20} cm^2 (∼1000−10 000 times lower than that of a dye molecule, ∼10^{-17}−10^{-16} cm^2).[13,14] This fundamental limitation impedes UCNPs in broadly harvesting infrared (IR) light and producing bright UCL, thus compromising their utility for a comprehensive range of applications.

Addressing the problem of spectrally narrow and low intensity absorption of lanthanide-doped UCNPs, Hummelen's group reported the design and synthesis of dye sensitized 10 nm $NaYF_4$:Yb^{3+}/Er^{3+} UCNPs in which excitation through absorption of the dye was realized.[15] However, a large energy mismatch between the donating energy level of the dye and the accepting energy level of Yb^{3+} ions resulted in an inefficient energy transfer between them. Moreover, the utilized $NaYF_4$:Yb^{3+}/Er^{3+} nanoparticles had to be devoid of any shell in order to allow dye sensitization to occur. Consequently, strong surface-related deactivations were manifested that typically lead to UCL quenching, two to three orders stronger than that for a core/shell structure with suppressed deactivations.[16] These limitations result in a very low upconversion quantum efficiency (UCQE) of ∼0.2% (calculated from conventional upconversion quantum yield of ∼0.1%),[15] meaning that merely ∼0.2% of the absorbed photons is upconverted into visible emission. The UCQE takes into consideration the conventional luminescence upconversion quantum yield (UCQY) and the order of photon processes involved in UCL (see Supporting Information Section G).[17,18]

Concept of Energy-Cascaded Upconversion. Herein, we introduce a new concept of energy-cascaded upconversion

(ECU), which exploits a hybrid inorganic−organic system consisting of an epitaxial core/shell upconverting nanocrystal and near-infrared (NIR) dyes anchored on the core/shell nanocrystal surface (Figure 1b). The NIR dyes can broadly and strongly harvest NIR light, and subsequently initialize multistep directional nonradiative energy transfer to excite lanthanide ions positioned within the inorganic core to entail an upconversion process. Specifically, the steps of excitation energy transfer can be classified as (1) from NIR-absorbing organic dyes across the organic/inorganic interface to type I lanthanide ions (intermediate sensitizers) incorporated at the shell layer; (2) from the intermediate sensitizers in the shell across the core/shell lattice interface to type II lanthanide ions (sensitizers) in the core domain; and (3) from the sensitizer ions to type III lanthanide ions (activators) within the host lattice of the core to produce upconversion via the classical ETU mechanism (Figure 1a). This multistep cascade energy transfer strategy, in which each step involves a small energy gap and provides for a maximum overlap between the emission of an energy donor and the absorption of an energy acceptor, leads to high efficiency for the transfer of harvested light energy all the way down to the upconverting lanthanide ions in the core. A hierarchical alignment of electronic energy levels (the NIR dye, the intermediate sensitizer, and the sensitizer), as depicted in Figure 1b, favors an unidirectional transfer of the harvested energy to lanthanide activators, preventing inverse energy transfer that couples to the nanoparticle surface to decrease the UCL efficiency. Moreover, because a core/shell design has been employed, surface-related UCL quenching in the core is significantly suppressed by the shell. As a consequence, energy-cascaded upconversion in dye-sensitized core/shell nanoparticles synergistically combines the merits of a core/shell nanocrystal structure and the "antenna" effect from the dye, producing ultrabright UCL under excitation in a broad spectral range. As a proof of concept demonstration, we utilize the design of NIR dye sensitized core/shell ($NaYbF_4$:Tm^{3+} 0.5%)@$NaYF_4$:Nd^{3+} nanoparticles, in which Nd^{3+} ions are doped in the shell layer as the type I lanthanide ions (intermediate sensitizers), whereas the Yb^{3+} and Tm^{3+} ions are corresponding type II (sensitizer) and type III (activator) lanthanide ions positioned in the core.

Design of Efficient Inorganic Fluoride Core/Shell Upconversion Nanocrystals. To realize high efficiency multistep energy-cascaded upconversion in a dye-sensitized core/shell structure, we first designed a core/shell nanocrystal of ($NaYbF_4$:Tm^{3+} 0.5%)@$NaYF_4$:Nd^{3+} and optimized nonradiative energy transfer from the Nd^{3+} in the shell to the Yb^{3+} ions in the core. We utilized $NaYbF_4$:Tm^{3+} 0.5% UCNPs as a core with known efficient energy transfer between Yb^{3+} and Tm^{3+} ions.[19] Monodispersed, hexagonal phase core/shell ($NaYbF_4$:Tm^{3+} 0.5%)@$NaYF_4$:Nd^{3+} x% nanoparticles of ∼54 nm size, with a shell thickness of ∼10 nm and x = 0−50% concentration of Nd^{3+} in the shell, were synthesized using a thermolysis procedure adapted from the literature (Supporting Information Section B).[3] The crystallographic phase, the formation of a core/shell structure, the dimensions of the core and the shell, as well as the stoichiometric composition have been substantiated by transmission electron microscopy (TEM), X-ray diffraction (XRD), energy dispersive X-ray spectra (EDX), and inductively coupled plasma mass spectrometry (ICP-MS) (Figure 1a, Supporting Information Figures S4−S6 and Table S3). The observation of new intense absorption peaks of Nd^{3+} ions (at 740, 800, and 860 nm) from

(NaYbF$_4$:Tm^{3+} 0.5%)@NaYF$_4$:Nd^{3+} 30% that are absent in (NaYbF$_4$:Tm^{3+} 0.5%)@NaYF$_4$ core/shell nanoparticles confirms successful incorporation of Nd^{3+} ions in the NaYF$_4$ shell layer (Supporting Information Figure S7). Core/shell nanoparticles of (NaYbF$_4$:Tm^{3+} 0.5%, Nd^{3+} 3%)@NaYF$_4$ were synthesized to examine the necessity of spatial isolation of the Yb^{3+}/Tm^{3+} ion combination from the Nd^{3+} ions (to prevent possible cross-relaxation between the Tm^{3+} and Nd^{3+} ions). Complete quenching of UCL was observed when the Nd^{3+} ions were doped into the core, in contrast to UCL from the (NaYbF$_4$:Tm^{3+} 0.5%)@NaYF$_4$:Nd^{3+} 3% core/shell UCNPs (Supporting Information Figure S8). This validates the rational design of incorporation of the Nd^{3+} ions into the shell and of the Yb^{3+}/Tm^{3+} ions into the core for high UCL, which at the same time grants an architecture for energy-cascaded upconversion.

The observed UCL in Figure 2b, when Nd^{3+} in the shell is excited at 800 nm, is the emission of Tm^{3+} peaked at: 340 nm
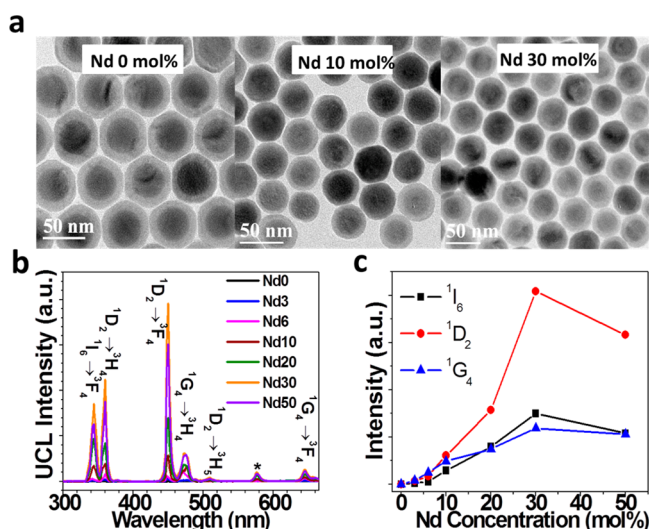

Figure 2. Design and characterizations of (NaYbF$_4$:Tm^{3+})@NaYF$_4$:Nd^{3+} core/shell UCNPs. (a) TEM images of the synthesized (NaYbF$_4$:Tm^{3+} 0.5%)@NaYF$_4$:Nd^{3+} x% (x = 0, 10, 30) core/shell nanoparticles. (b) The UCL spectra of the colloidal (NaYbF$_4$:Tm^{3+} 0.5%)@NaYF$_4$:Nd^{3+} x% (x = 0, 3, 6, 10, 20, 30, 50) core/shell nanoparticles dispersed in hexane. Absorption of Yb^{3+} ion in all Nd^{3+}-doped core/shell UCNPs were matched at ~980 nm to ensure an identical nanoparticle concentration for comparison (Supporting Information Figure S9). Excitation at 800 nm with a power density of 10 W/cm^2. (c) Dependence of the UCL intensities from the $^1I_6$, $^1D_2$, and $^1G_4$ states, on the Nd^{3+} concentration in the colloidal (NaYbF$_4$:Tm^{3+} 0.5%)@NaYF$_4$:Nd^{3+} x% core/shell UCNPs. The emissions peaked at 340 nm ($^1I_6 \rightarrow {}^3F_4$), and at 350, 450, and 510 nm (from $^1D_2$ state to $^3H_6$, $^3F_4$, and $^3H_5$ states), as well as at 480 and 650 nm (from $^1G_4$ to $^3H_6$ and $^3F_4$), were integrated to obtain the value of the overall emission intensities from the $^1I_6$, $^1D_2$, and $^1G_4$ states, respectively.

(from the $^1I_6$ state, five-photon process); 350, 450, and 510 nm (from the $^1D_2$ state, four-photon process); and 480 and 660 nm (from the $^1G_4$ state, three-photon process).[20] The number of photons was determined from the dependence of the luminescence intensities on the laser excitation power density (Supporting Information Figure S35). The UCL intensities from the $^1I_6$, $^1D_2$, and $^1G_4$ states of Tm^{3+} ions, all have a similar dependence on the Nd^{3+} concentration, reaching maximum at the Nd^{3+} concentration of 30% (Figure 2b and 2c). In analogy

to UCL, the concurrent downconversion luminescence (DCL) from the Yb^{3+} ions is also dependent on the Nd^{3+} concentration (Supporting Information Figure S10). These dependences illustrate that the Nd^{3+} ions in the shell transfer excitation energy to the Yb^{3+} ions, which in turn sensitize the Tm^{3+} ions in the core. This conclusion is supported by the excitation spectra of UCL from the $^1I_6$, $^1D_2$, and $^1G_4$ states of Tm^{3+} ions in the NaYbF$_4$:Tm^{3+}@NaYF$_4$:Nd^{3+} 30% core/shell UCNPs (Supporting Information Figure S11). The observed UCL excitation peaks match the absorption peaks of the Nd^{3+} ions at 740, 800, and 860 nm, and the one of Yb^{3+} ions at 980 nm. Another evidence of energy transfer from Nd^{3+} in the shell to Yb^{3+} in the core was further provided by the luminescence spectra of the core/shell UCNPs without Tm^{3+} (NaYF$_4$@NaYF$_4$:Nd^{3+} 3% and NaYF$_4$:Yb^{3+} 30%@NaYF$_4$:Nd^{3+} 3%) (Supporting Information Figure S12). The possible upconverting pathways in NaYbF$_4$:Tm^{3+}@NaYF$_4$:Nd^{3+} core/shell UCNPs are described in Figure 3d, when exciting Nd^{3+} directly. An optimized UCL intensity at Nd^{3+} concentration of 30% arises from the competition between two parallel processes. One is to harvest light at ~800 nm and then transfer the harvested energy to Yb^{3+} ions. A high concentration of Nd^{3+} should favors the UCL process due to the increased absorption cross section of the core/shell nanoparticle as well as the elevated energy transfer rate from Nd^{3+} to Yb^{3+} ions. The other one is the detrimental cross relaxation process between the Nd^{3+} ions ($^4F_{3/2} + {}^4I_{9/2} \rightarrow 2{}^4I_{15/2}$), which deactivates the harvested energy of Nd^{3+} ions (Figure S15 in the revised Supporting Information) and also increases with the increase of the Nd^{3+} concentration. A balanced effect might occur at an optimized Nd^{3+} concentration of 30%; increasing Nd^{3+} concentration over this value will make the detrimental effect surpass the beneficial effect, thus leading to the decrease of UCL.

Utilization of the Yb^{3+}-enriched NaYbF$_4$ host lattice as a core not only favors high UCL from Tm^{3+},[19] but also facilitates the Nd^{3+} (shell) → Yb^{3+} (core) energy transfer process. The efficiency of a nonradiative energy transfer can be quantified using the following equation[21]

$$ET = 1 - \frac{\tau_{DA}}{\tau_D} \qquad (1)$$

where ET stands for energy transfer efficiency, whereas τ_D and the τ_{DA} are the effective lifetimes of the energy donor in the absence and the presence of an energy acceptor, respectively. Following this equation and measuring decays of DCL from the Nd^{3+} ions, the energy transfer efficiency was determined to be ~39% and ~66% for (NaYF$_4$:Yb^{3+})@NaYF$_4$:Nd^{3+} 3% UCNPs containing 30% and 100% Yb^{3+} ions in the core, respectively (Supporting Information Figure S13). This result confirms the importance of using an Yb^{3+}-enriched NaYbF$_4$ host lattice as a core to produce efficient Nd^{3+} (shell) → Yb^{3+} (core) energy transfer. For the UCL-optimized core/shell nanoparticles of NaYbF$_4$:Tm^{3+} 0.5%@NaYF$_4$:Nd^{3+} 30%, the energy transfer efficiency was determined to be as high as ~80% (Supporting Information Figure S14), despite an existence of the detrimental cross relaxation process between the Nd^{3+} ions ($^4F_{3/2} + {}^4I_{9/2} \rightarrow 2{}^4I_{15/2}$, Supporting Information Figure S15).[22]

The integrated intensity of multiphoton UCL from the optimized (NaYbF$_4$:Tm^{3+} 0.5%)@NaYF$_4$:Nd^{3+} 30% UCNPs was found to be six times higher, when excited at ~980 nm, than that from the canonical ~30 nm sized NaYF$_4$:Yb^{3+} 30%, Tm^{3+} 0.5%@NaYF$_4$ core/shell nanoparticles, indicating
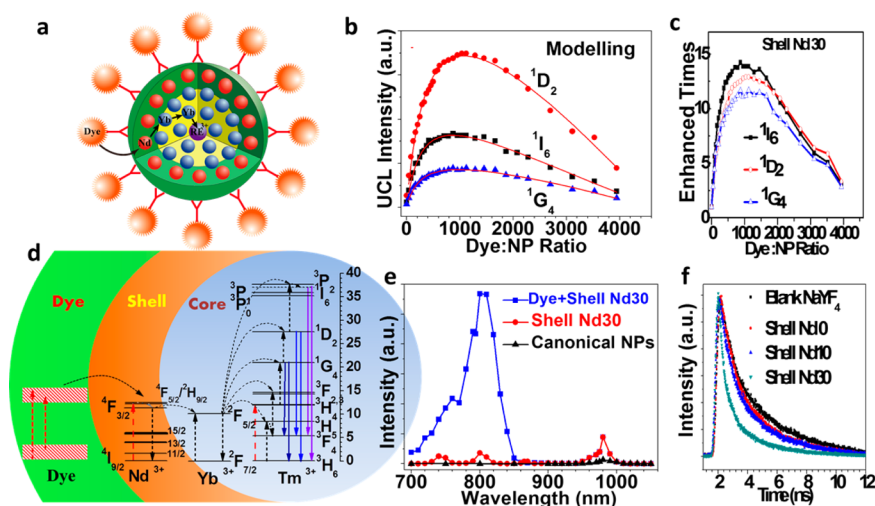
Figure 3. Energy-cascaded upconversion in dye-sensitized fluoride core/shell nanocrystals. (a) Scheme of the proposed nanostructure. (b) UCL intensities from the $^1I_6$, $^1D_2$, and $^1G_4$ states of Tm^{3+} as a function of the number ratio of IR-808 dye: NP for the $(NaYbF_4:Tm^{3+}\ 0.5\%)@NaYF_4:Nd^{3+}$ 30% UCNPs. Excitation at 800 nm, 10 W/cm². (c) Dependencies of UCL enhancement in the $(NaYbF_4:Tm^{3+}\ 0.5\%)@NaYF_4:Nd^{3+}$ 30% UCNPs on the number ratio of IR 808 dye: NP for the $(NaYbF_4:Tm^{3+}\ 0.5\%)@NaYF_4:Nd^{3+}$ 30% UCNPs. The enhancement time is defined compared to the core/shell UCNPs without dye. Excitation at 800 nm, 10 W/cm². (d) Proposed energy transfer pathways in the dye-sensitized core/shell structure. The higher energy levels of Nd^{3+} are omitted, as no UCL from the Nd^{3+} ions is observed. The dye molecules on the core/shell nanoparticle surface absorb photons and transfer excitation energy to the Nd^{3+} ions in the shell, which in turn sensitize Yb^{3+} ions in the core. Subsequently, intracore energy transfer from Yb^{3+} to Tm^{3+} excites the Tm^{3+} ions from the ground state to the $^1G_4$, $^1D_2$, and the $^1I_6$ states. Radiative decays from these states produce five-photon induced UCL at 340 nm ($^1I_6 \rightarrow {}^3F_4$), four-photon induced UCL at 350, 450, and 510 nm (from $^1D_2$ state to $^3H_6$, $^3F_4$, and $^3H_5$ states), as well as three-photon luminescence at 480 and 650 nm (from $^1G_4$ to $^3H_6$ and $^3F_4$). (e) UCL excitation spectra (for the integrated UCL intensity from the $^1D_2$ state) for: IR-808 dye-sensitized $(NaYbF_4:Tm^{3+}\ 0.5\%)@NaYF_4:Nd^{3+}$ 30% (blue), $(NaYbF_4:Tm^{3+}\ 0.5\%)@NaYF_4:Nd^{3+}$ 30% (red), and canonical $(NaYF_4:Yb^{3+}\ 30\%,Tm^{3+}\ 0.5\%)/NaYF_4$ core/shell UCNPs (black). The broad and intense UCL excitation band peaked at ∼800 nm proves the sensitization of the UCL by the IR-808 dye. (f) Fluorescence decay of the IR-808 dye from the IR-808 sensitized "blank" $NaYF_4$ nanoparticles as well as the $(NaYbF_4:Tm^{3+}\ 0.5\%)@NaYF_4$, $(NaYbF_4:Tm^{3+}\ 0.5\%)@NaYF_4:Nd^{3+}$ 10%, and the $(NaYbF_4:Tm^{3+}\ 0.5\%)@NaYF_4:Nd^{3+}$ 30% core/shell nanoparticles.

successful suppression of surface-related quenching mechanisms and the importance of high Yb^{3+} content in the core for achieving intense UCL (Supporting Information Figures S16 and S17).[23] When excited at ∼800 nm, the integrated UCL from our optimized core/shell UCNPs is evaluated to be about ∼41 times more intense than that from the $(NaYF_4:Yb^{3+}\ 20\%$, $Tm^{3+}\ 0.5\%$, $Nd^{3+}\ 1\%)@NaYF_4:Nd^{3+}$ 20% core/shell nanoparticles that have recently been reported as highly efficient UCNPs (Supporting Information Figure S18).[24,25] The UCQE of our optimized $(NaYbF_4:Tm^{3+}\ 0.5\%)@NaYF_4:Nd^{3+}$ 30% core/shell UCNPs was determined to be about ∼8.7% (UCQY is of 2.4%, upconversion energy conversion efficiency of 4.4%) when excited at 800 nm with 10 W/cm² (Supporting Information Figure S34), which is about 40 times higher than 0.22% (UCQY of 0.11%), the highest value reported up to date for nanoparticles with UC induced by Nd^{3+} absorption (core/shell/shell nanostructure of $NaYF_4:Yb^{3+}\ 20\%$, $Er^{3+}\ 2\%@NaYF_4:Yb^{3+}\ 10\%@NaNdF_4:Yb^{3+}\ 10\%$, excited at 800 nm with 20 W/cm²).[26] We attribute such a dramatic increase in UC efficiency to highly efficient energy transfer between Nd^{3+} in the shell and Yb^{3+} in the core, along with that between Yb^{3+} and Tm^{3+} within the core.

Energy-Cascaded Upconversion in Organic Dye-Sensitized Core/Shell Fluoride Nanocrystals. Nucleophilic substitution of the central chlorine atom in commercial IR-783 was used to prepare a carboxylic acid-functionalized derivative, coined as the IR-808 dye (see Supporting Information Scheme S1). The main absorption band of IR-808 is between 650 and 850 nm, with a maximum at 808 nm in DMF (Supporting Information Figure S19); dye mass extinction coefficient is 12.7

l g⁻¹ cm⁻¹, which is ∼3000 times higher than that of the optimized $(NaYbF_4:Tm^{3+}\ 0.5\%)@NaYF_4:Nd^{3+}$ 30% core/shell nanoparticles at a peaked absorption wavelength of 794 nm (4.2×10^{-3} l g⁻¹ cm⁻¹) (Supporting Information Table S4). Negligible absorption of IR-808 below 650 nm is essential for the experiment, as the antenna dye should be transparent to the upconverted photons emitted by the nanoparticle (Supporting Information Figure S19). The emission spectrum of IR-808 overlaps strongly with the absorption peaks of Nd^{3+} in the shell and with that of the Yb^{3+} in the core of the $(NaYbF_4:Tm^{3+}\ 0.5\%)@NaYF_4:Nd^{3+}$ 30% core/shell nanoparticles (Supporting Information Figure S20). This overlap allows for nonradiative energy transfer from IR-808 to the Nd^{3+} ions in the shell and possibly to the Yb^{3+} ions in the core. A broad spectroscopic range (760−830 nm) of light excitation induced the same luminescence spectra of IR-808 (Supporting Information Figure S21). This spectroscopic behavior entails an identical mechanism of nonradiative energy transfer from IR-808 to doped trivalent lanthanides despite excitation at distinct wavelengths.

To produce a close contact between the IR-808 dye and the core/shell nanoparticle, a very short ionic $NOBF_4^-$ ligand was first used to replace the original oleic ligand, following a protocol from the literature,[27] and then further exchanged with the carboxylic-functionalized IR-808 dye. The success of ligand exchange in each step has been confirmed by the measured Fourier transform infrared (FTIR) spectra of involved samples (Supporting Information Figure S22). Attachment of IR-808 to the surface of the core/shell UCNPs was also clearly confirmed by changes in the spectral properties of the dye (Supporting

Information Figures S23−S25). First, the emission peak for IR-808 attached to the core/shell UCNPs (dispersed in DMF) was shifted from 854 to 849 nm (Supporting Information Figure S23). At the same time, the absorption maximum wavelength of IR-808 in the dye-attached upconverting nanoparticles was blue-shifted from 808 to 804 nm (Supporting Information Figure S24). Second, fluorescence anisotropy measurement showed an apparent difference between a suspension of the dye attached to core/shell UCNPs and a free IR-808 solution, clearly revealing the binding of IR-808 to the surface of the nanoparticles (Supporting Information Figure S25). The attachment of the IR 808 dye to the nanoparticle surface is a complex process, involving three possible mechanisms that include electrostatic interaction, physical adsorption, and chemical coordination interaction. For chemical coordination mechanism, both the carboxylic acid and the sulfate groups of IR 808 dye can contribute to its anchoring to the nanoparticle surface (as confirmed by the FTIR spectra shown in Supporting Information Figure S22). The orientation of the dye molecules on the surface is difficult to ascertain but is supposed to be approximately parallel to the nanoparticle surface when chemical coordination plays the dominant role.

The possibility of energy transfer from IR 808 to the Nd^{3+} ions was experimentally verified through dye sensitization of pure Nd^{3+} doped $NaYF_4$ nanoparticles, whereby luminescence from the Nd^{3+} ions was enhanced 33 times at an optimal dye concentration (Supporting Information Figure S26). We then tested the energy-cascaded upconversion by exploring the energy transfer pathways depicted in Figures 3a and 3d, that is, dye → Nd (in the shell) → Yb (in the core) → Tm (in the core), using a range of Nd^{3+}-sensitized core/shell structures described in Figure 2. When introducing varied concentrations of the IR 808 dye into these core/shell nanoparticle dispersions (in DMF), the UCL intensities from the $^1I_6$, $^1D_2$, and $^1G_4$ states exhibit a strong dependence on the dye: NP ratio (Figure 3b and c, Supporting Information Figure S27 for core/shell UCNPs with varied Nd^{3+} concentrations of 8−50% in the shell). The UCL intensities were all enhanced by more than 1 order of magnitude, when excited at 10 W/cm^2 at 800 nm; for example, the UCL from the optimized $(NaYbF_4:Tm^{3+}$ 0.5%)@$NaYF_4:Nd^{3+}$ 30% core/shell UCNPs were enhanced 14-fold (Figure 3c). We found that the photostability of the dye associated with UCNPs is similar to that of the free dye (Supporting Information Figure S28). It is worth noting that the nonlinear nature of upconversion makes the enhancement effect become much more pronounced at lower excitation density range (Supporting Information Figure S29).[28] The UCL boost is also visible from the photographic images of UCNPs dispersions with and without the dye (Supporting Information Figure S30). These enhancement results verify the antenna effect provided by the dye attached to the core/shell nanoparticle surface. To confirm this, the excitation spectra for the upconversion emission from the $^1D_2$ state (Figure 3e) as well as from the $^1I_6$ and $^1G_4$ states (Supporting Information Figure S31) were measured for the IR-808-sensitized in comparison to pure $(NaYbF_4:Tm^{3+}$ 0.5%)@$NaYF_4:Nd^{3+}$ 30% core/shell nanoparticles. A broad, intense band between 700 and 850 nm was clearly observed for the dye-sensitized UCNPs, in marked contrast to the narrow and weak peaks of Nd^{3+} ions at 800 and 860 nm for the nanoparticles without dye sensitization. Moreover, the shape of this broad excitation band exactly matches the absorption band of IR-808, clearly

demonstrating that the antenna effect stems from the dye (Supporting Information Figure S31).

The dye antenna effect can take place through two mechanisms of energy transfer: (i) radiative type and (ii) nonradiative type. A linear dependence of the UCL intensity on the diluted concentrations of the dye-sensitized core/shell UCNPs rules out the radiative type mechanism (Supporting Information Figure S32). Moreover, we acquired the decay of fluorescence of the IR-808 bound to the surface of the $(NaYbF_4:Tm^{3+}$ 0.5%)@$NaYF_4:Nd^{3+}$ (0, 10, and 30%) core/shell nanoparticles (Figure 3f). The average lifetime of IR-808 fluorescence was gradually shortened with an increase of the Nd^{3+} concentration in the shell, from 2.10 ns (IR-808 for the blank $NaYF_4$ nanoparticle) to 1.80, 1.62, and 0.37 ns for the shell Nd^{3+} concentration of 0, 10, and 30%, respectively. This shortening of fluorescence lifetime confirms a nonradiative type of energy transfer from the IR-808 dye to Nd^{3+}, whereas the decreasing decay trend reveals the important impact of the Nd^{3+} concentration to enhance the energy transfer efficiency. The maximal efficiency of nonradiative energy transfer was determined to be about ∼82% for the optimized core/shell UCNPs doped with 30% Nd^{3+} in the shell. Though nonradiative energy transfer from IR-808 to Nd^{3+} might take place through a Föster-type or a Dexter-type mechanism,[29] we believe that the long-range Förster type is more likely to occur because of the unchanged spin associated with the energy transfer, as well as the distance between the dye and the Nd^{3+} ion, defined by the geometric size of the IR-808 dye (∼2 nm) and a random distribution of the Nd^{3+} ion in a 10 nm thick shell. Moreover, the energy gap is ∼170 cm^{-1} between the singlet electronic excitation level of the IR-808 dye and the $^4F_{5/2}/^2H_{9/2}$ level of Nd^{3+}, and 990 cm^{-1} between the $^4F_{3/2}$ level of Nd^{3+} and the $^2F_{5/2}$ level of Yb^{3+}, whereas the energy gap between the NIR dye and Yb^{3+} is 2200 cm^{-1}. According to these energy gaps as well as pertinent optical parameters, we calculated that multistep cascade energy transfer (from the dye to Nd^{3+}, and then to Yb^{3+}) can be about 1.5 times more efficient than a direct energy transfer from the IR-808 dye to the Yb^{3+} ions (Supporting Information Section J1). Moreover, the Förster radius was determined to be ∼1.9 nm, and the actual distance between the IR-808 dye and the Nd^{3+} ions was estimated to be ∼1.5 nm according to the measured energy transfer efficiency (∼80%), indicating a close contact between the dye and the inorganic core/shell nanoparticle surface (Supporting Information Section J1).

As illustrated in Figure 3b and c, the luminescence intensities from the $^1I_6$, $^1D_2$, and $^1G_4$ states all increase first with the increased dye: NP ratio, which is consistent with increasing overall absorption of the excitation energy at 800 nm by an increasing number of surface-bound antenna molecules. However, beyond a certain concentration, a further increase of the IR-808/nanoparticle ratio results in decreased luminescence intensities. The observed decline can be explained by two factors: increased mutual interactions between the antenna molecules on the core/shell nanoparticle surface (self-quenching) and an increasing concentration of unbound (excess) antenna molecules which absorb the excitation energy but do not transfer it to the nanoparticles. We theoretically modeled the kinetics to interpret the dependence of the UCL intensities from the $^1I_6$, $^1D_2$, and $^1G_4$ states on the IR-808 dye concentration under an extreme saturation excitation regime as in the case shown in Figure 3b, where the intensity of UCL is proportional to the excitation power density (Supporting
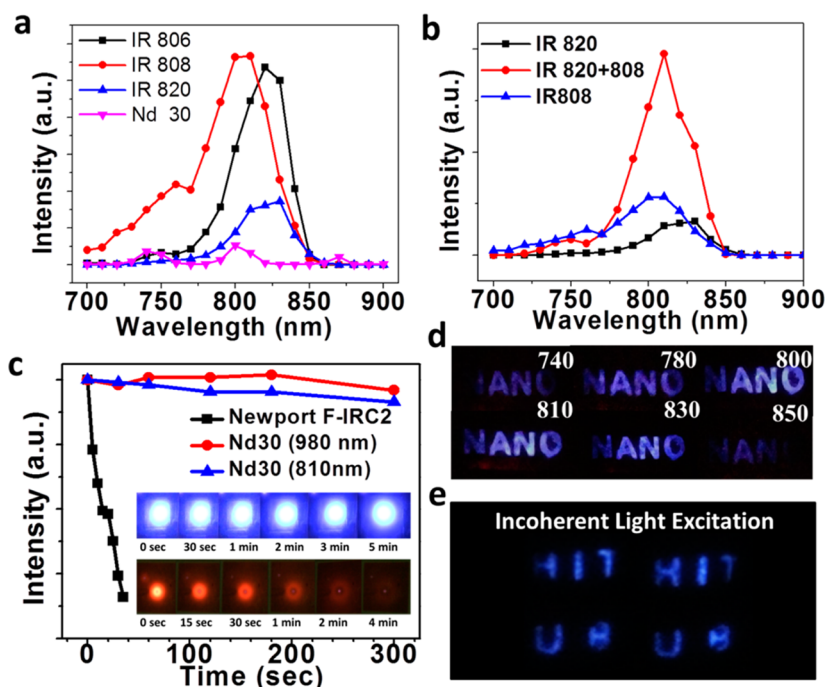
Figure 4. Co-sensitization and applications of an inorganic fluoride core/shell nanostructure. (a) Excitation spectra of UCL peaked at 350 nm from the core/shell (NaYbF$_4$:Tm^{3+} 0.5%)@NaYF$_4$:Nd^{3+} 30% nanoparticles (Nd 30) as well as from the IR 808-sensitized (IR 808), the IR 806-sensitized (IR 806), and the IR 820-sensitized (IR 820) core/shell (NaYbF$_4$:Tm^{3+} 0.5%)@NaYF$_4$:Nd^{3+} 30% nanoparticles. (b) Excitation spectra of UCL peaked at 350 nm from IR 808-sensitized, IR 820-sensitized, as well as the IR 808 and IR 820-co-sensitized core/shell (NaYbF$_4$:Tm^{3+} 0.5%)@NaYF$_4$:Nd^{3+} 30% nanoparticles. An exact amount of IR 808 and IR 820 is utilized for the co-sensitization experiment as the one used for single dye sensitization. (c) Photostability of UCL from a homemade IR card and a commercial IR card (Newport F-IRC2, Irvine, CA) excited at 810 nm, 1 W/cm^2. The inset shows the photographic images of both cards taken at different time points. The photostability of UCL from homemade IR card excited at ∼980 nm is shown as a reference (1 W/cm^2). As laser photons at ∼980 nm directly act on the Yb^{3+} ions to excite the Yb^{3+}/Tm^{3+} ion pairs for upconversion, no photobleaching exists under this excitation condition. (d) Blue upconversion from regular letters printed using an upconverting ink made by the IR-808-sensitized (NaYbF$_4$:Tm^{3+} 0.5%)@NaYF$_4$:Nd^{3+} core/shell nanoparticles and polystyrene. (e) Upconversion of incoherent light (halogen lamp) by the IR-808 and IR-820 co-sensitized (NaYbF$_4$:Tm^{3+} 0.5%)@NaYF$_4$:Nd^{3+} core/shell nanoparticles (0. 016 W/cm^2). A long pass optical filter was used to cut off light below 750 nm.

Information Figure S35).[27] We consider the following dynamic process to model: laser excitation of the dye, radiative and nonradiative deexcitation of the dye in the excited state, concentration quenching of the dye in the excited state, energy transfer from the dye to the Nd^{3+}, the back energy transfer from the Nd^{3+} to the dye, radiative and nonradiative deactivation of Nd^{3+} in the excited state, as well as concentration quenching of Nd^{3+} in the excited state (see Supporting Information Section J2). Our kinetic modeling results reveal that self-quenching of the antenna dyes is the main mechanism to decrease UCL at high concentrations, agreeing well with all measured experimental data (Figure 3b).

The optimum dye:NP number ratio was determined to be ∼830 (corresponding to an optimum weight ratio of 1:304); this means that a mean of ∼830 antenna molecules (absorption cross section, 1.84 × 10^{-17} cm^2) is bound to the surface of per (NaYbF$_4$:Tm^{3+} 0.5%)@NaYF$_4$:Nd^{3+} 30% core/shell nanoparticle (absorption cross section, 1.48 × 10^{-15} cm^2) at this ratio; the intermolecular distance of dyes is estimated to be ∼3 nm, that is close to the length scale of the IR-808 dye (∼2 nm) (Supporting Information Section F). The absorption cross section of a single dye-bound core/shell nanoparticle is calculated to be as large as 1.48 × 10^{-14} cm^2 (in good agreement with the experiment-determined value of 1.47 × 10^{-14} cm^2), which is about 10 times higher than that of a single (NaYbF$_4$:Tm^{3+} 0.5%)@NaYF$_4$:Nd^{3+} 30% core/shell nano-

particle, and ∼1000 times higher than a single organic dye molecule (absorption cross section, ∼10^{-17} cm^2).

The optimized UCL from the IR-808 dye-sensitized (NaYbF$_4$:Tm^{3+} 0.5%)@NaYF$_4$:Nd^{3+} 30% core/shell UCNPs was shown to be ∼14 times higher than that of (NaYbF$_4$:Tm^{3+} 0.5%)@NaYF$_4$:Nd^{3+} 30% UCNPs without the dye, 658 times higher than the reported highly efficient (NaYF$_4$:Yb^{3+} 20%, Tm^{3+} 0.5%, Nd^{3+} 1%)@NaYF$_4$:Nd^{3+} 20% core/shell nanoparticles,[24] and more than 40 000 times higher than that of the (NaYbF$_4$:Tm^{3+} 0.5%)/NaYF$_4$ nanoparticles when excited at ∼800 nm (10 W/cm^2) (Supporting Information Figure S33). Moreover, the intensity of UCL from the ^{1}D$_2$ state (∼350 nm) in the IR 808 dye-sensitized core/shell structure, when excited at 800 nm, is about 25 times higher than that from the canonical core/shell nanoparticles of the hexagonal phase (NaYF$_4$:Yb^{3+} 30%, Tm^{3+} 0.5%)/NaYF$_4$ (size, 30 nm), when excited at ∼980 nm using the same laser power (Figure 3e).[23] The UCQE of the optimized IR 808 dye-sensitized (NaYbF$_4$:Tm^{3+} 0.5%)@NaYF$_4$:Nd^{3+} 30% core/shell nanocrystals was evaluated to be as high as 19% (upconversion energy conversion efficiency 9.3%, UCQY 4.8%;) when excited at ∼800 nm with 10 W/cm^2 (Supporting Information Figure S34). This UCQE is also comparable to the highest reported one of 22% up to date for two-photon blue upconversion via organic triplet−triplet annihilation (∼450 nm emission, excited at ∼532 nm).[30] This value is higher than that from the (NaYbF$_4$:Tm^{3+} 0.5%)@NaYF$_4$:Nd^{3+} 30% core/shell nano-

particles, dye-sensitized ($NaYbF_4$:Tm^{3+} 0.5%)@$NaYF_4$ core/shell nanoparticles, and the dye-sensitized $NaYbF_4$:Tm^{3+} 0.5% nanoparticles (Supporting Information Figure S34). In addition, we show that energy-cascaded upconversion is not limited to the type of inorganic host lattice employed here to build a core/shell structure (Supporting Information Figure S36), to the type of organic dyes employed to sensitize (Figure 4a), or to the type of activator utilized here to produce UCL (Supporting Information Figures S37 and S38), extending the proposed concept to a general type of dye-sensitized inorganic core/shell nanostructures.

Co-Sensitization and Applications of Dye-Sensitized Core/Shell Fluoride Nanocrystals. Along with IR-808, we showed that the commercially available IR dyes of IR-806 and IR-820 can sensitize ($NaYbF_4$:Tm^{3+} 0.5%)@$NaYF_4$:Nd^{3+} 30% core/shell nanoparticles to create energy-cascaded upconversion (Figure 4a). A simultaneous use of the IR-808 and the IR-820 dyes is able to produce a pronounced co-sensitizing antenna effect, which synergistically adds up the sensitization effect from each type of the involved dyes (Figure 4b). The dye co-sensitizing results provides an opportunity to produce a comprehensive IR harvesting spectral range for energy-cascaded upconversion through simultaneous use of a set of IR dyes that possess varying absorption spectra.

A broad spectral response as well as a high UCQE promises the use of dye-sensitized ($NaYbF_4$:Tm^{3+} 0.5%)@$NaYF_4$:Nd^{3+} 30% UCNPs in many applications. A straightforward application is visualization of a broad spectrum of invisible IR lasers. In fact, under excitation in the spectral range of 720−870 nm, blue UCL can be viewed by naked eye, from the IR-808 and IR-820 co-sensitized ($NaYbF_4$:Tm^{3+} 0.5%)@$NaYF_4$:Nd^{3+} 30% UCNPs in DMF and in our homemade IR card (Supporting Information Figure S39). In addition to this broad spectral response provided by IR dye sensitization, direct excitation of Yb^{3+}/Tm^{3+} ions provides another spectral IR range of 920−1000 nm for visualizing via upconversion (Supporting Information Figure S40). We also compared the performance of our homemade IR card with that of a commercial IR card (Newport F-IRC2) under identical laser irradiance. As illustrated in Figure 4c, visible yellow luminescence from the commercial Newport IR card disappears after less than 20 s of illumination, whereas blue UCL from our homemade IR card exhibits a slight reduction of ∼10% after 300 s of irradiation, which is apparently associated with dye photobleaching. As such, the necessity of frequent movement of a commercial IR card for visualization of lasers is eliminated when using homemade IR card containing dye-sensitized core/shell nanoparticles.

As a proof-of-concept demonstration of security applications of dye-sensitized core/shell nanoparticles, regular letters were printed using an invisible ink-like suspension, formulated by a mixture of IR-808-sensitized UCNPs and visibly transparent polystyrene polymer. These secured printed semitransparent letters appear to be slightly visible, with low contrast letters for the naked eye, but turn into high contrast blue letters when irradiated with a multitude of IR wavelengths in the range of 730−980 nm (Figure 4d, and Supporting Information Figure S40). The ability to utilize numerous excitation IR wavelengths for decoding provides strong potential for wide use of IR-808-sensitized core/shell UCNPs for security purpose. Moreover, we demonstrated that low power incoherent light from a conventional light source can be utilized to excite IR-808 and IR-820 co-sensitized core/shell UCNPs, producing adequate

UCL for visualization (Figure 4e). Clear letters with blue upconversion (three photon process) can be seen and captured by an iPhone 5s camera, even with an excitation power density of 0.016 W/cm² in the spectral range of 750−1100 nm. It should be noted that this level of power density is comparable with sun power density at Earth's surface (∼0.0163 W/cm² of average power density and whole spectrum; sun power density at the equator can be as high as 0.1 W/cm²). According to our knowledge, this is the first demonstration of incoherent light induced three-photon upconversion. This highly efficient upconversion can have important implications in many fields (e.g., to increase the efficiency via circumventing IR transmission losses in solar cells and to visualize NIR light in night vision devices).

Conclusion. We have introduced and validated a concept of energy-cascaded upconversion using NIR dye sensitized ($NaYbF_4$:Tm^{3+} 0.5%)@$NaYF_4$:Nd^{3+} core/shell nanoparticles as a model. Broadly absorbing infrared dyes are able to efficiently harvest irradiation energy, which is nonradiatively transferred to the Nd^{3+} ions in the shell (efficiency, 82%) and, sequentially, to the Yb^{3+} ions in the core (efficiency, 80%) that sensitize Tm^{3+} ions positioned also in the core to produce multiphoton UCL. This multistep energy-cascaded transfer enables an upconversion quantum efficiency as high as 19% (upconversion energy conversion efficiency of 9.3%, upconversion quantum yield of 4.8%), a broad NIR excitation response range over 150 nm (700−850 nm), along with a large absorption cross section of 1.47×10^{-14} cm² per single dye-sensitized core/shell nanoparticle. This energy-cascaded upconversion can be applied to a set of different IR dyes and lanthanide emitters, as well as to other fluoride host lattices. The utilization of dye-sensitized core/shell nanoparticles for several applications (IR laser detection, security decoding, as well as incoherent light upconversion) was demonstrated, with implications for a broad spectrum of photonic applications.

■ ASSOCIATED CONTENT

Ⓢ Supporting Information

The Supporting Information is available free of charge on the ACS Publications website at DOI: 10.1021/acs.nanolett.5b02830.

> Chemicals and instrumentation, synthetic procedures, sample preparations, supporting figures for core/shell nanostructures, supporting figures for IR dye-sensitized core/shell nanostructures, estimations of molecular weights, number of dyes per core/shell nanoparticle, and intermolecular distance of IR dye on the surface of a core/shell nanoparticle, quantification of upconversion quantum efficiency, pump power dependence, supporting figures for generalization of dye-sensitized core/shell structure, supporting figures for applications, and the theoretical modeling. (PDF)

■ AUTHOR INFORMATION

Corresponding Authors
*E-mail: pnprasad@buffalo.edu.
*E-mail: chenguanying@hit.edu.cn.

Author Contributions

G.C. conceived the idea and designed all pertinent experiments. J.D. and W.S. synthesized inorganic core/shell nanoparticles; G.C., H.Q., and W.S. obtained dye-sensitization results; T.Y.O. contributed to the idea development and design the spectros-

copy experiments and took part in the spectral measurements as well as in demonstration of incoherent light upconversion; R.R.V. and H.Å. did theoretical modeling; X.W. and G.H. synthesized IR-808 dyes, Y.W. measured lifetimes of IR dyes; G.C. and T.Y.O. prepared the manuscript, and all authors discussed and commented on the manuscript. G.C. and P.N.P. directed the project.

Notes

The authors declare no competing financial interest.

■ REFERENCES

(1) Chen, G. Y.; Qiu, H. L.; Prasad, P. N.; Chen, X. Y. Upconversion Nanoparticles: Design, Nanochemistry, and Applications in Theranostics. *Chem. Rev.* **2014**, *114* (10), 5161−5214.

(2) Wang, F.; Han, Y.; Lim, C. S.; Lu, Y. H.; Wang, J.; Xu, J.; Chen, H. Y.; Zhang, C.; Hong, M. H.; Liu, X. G. Simultaneous phase and size control of upconversion nanocrystals through lanthanide doping. *Nature* **2010**, *463* (7284), 1061−1065.

(3) Mai, H. X.; Zhang, Y. W.; Si, R.; Yan, Z. G.; Sun, L. D.; You, L. P.; Yan, C. H. High-quality sodium rare-earth fluoride nanocrystals: Controlled synthesis and optical properties. *J. Am. Chem. Soc.* **2006**, *128* (19), 6426−6436.

(4) Li, Z. Q.; Zhang, Y. An efficient and user-friendly method for the synthesis of hexagonal-phase NaYF₄: Yb, Er/Tm nanocrystals with controllable shape and upconversion fluorescence. *Nanotechnology* **2008**, *19* (34), 5.

(5) Deng, R. R.; Qin, F.; Chen, R. F.; Huang, W.; Hong, M. H.; Liu, X. G. Temporal full-colour tuning through non-steady-state upconversion. *Nat. Nanotechnol.* **2015**, *10* (3), 237−242.

(6) Zhao, J. B.; Jin, D. Y.; Schartner, E. P.; Lu, Y. Q.; Liu, Y. J.; Zvyagin, A. V.; Zhang, L. X.; Dawes, J. M.; Xi, P.; Piper, J. A.; Goldys, E. M.; Monro, T. M. Single-nanocrystal sensitivity achieved by enhanced upconversion luminescence. *Nat. Nanotechnol.* **2013**, *8* (10), 729−734.

(7) Gargas, D. J.; Chan, E. M.; Ostrowski, A. D.; Aloni, S.; Altoe, M. V. P.; Barnard, E. S.; Sanii, B.; Urban, J. J.; Milliron, D. J.; Cohen, B. E.; Schuck, P. J. Engineering bright sub-10-nm upconverting nanocrystals for single-molecule imaging. *Nat. Nanotechnol.* **2014**, *9* (4), 300−305.

(8) Li, X. M.; Wang, R.; Zhang, F.; Zhao, D. Y. Engineering Homogeneous Doping in Single Nanoparticle To Enhance Upconversion Efficiency. *Nano Lett.* **2014**, *14* (6), 3634−3639.

(9) Yi, G. S.; Chow, G. M. Water-soluble NaYF₄:Yb,Er(Tm)/NaYF₄/polymer core/shell/shell nanoparticles with significant enhancement of upconversion fluorescence. *Chem. Mater.* **2007**, *19* (3), 341−343.

(10) Vetrone, F.; Naccache, R.; Mahalingam, V.; Morgan, C. G.; Capobianco, J. A. The Active-Core/Active-Shell Approach: A Strategy to Enhance the Upconversion Luminescence in Lanthanide-Doped Nanoparticles. *Adv. Funct. Mater.* **2009**, *19* (18), 2924−2929.

(11) Wu, D. M.; Garcia-Etxarri, A.; Salleo, A.; Dionne, J. A. Plasmon-Enhanced Upconversion. *J. Phys. Chem. Lett.* **2014**, *5* (22), 4020−4031.

(12) Carnall, W. T.; Goodman, G. L.; Rajnak, K.; Rana, R. S. A Systematic Analysis of the Spectra of the Lanthanides Doped into Single-Crystal LaF₃. *J. Chem. Phys.* **1989**, *90* (7), 3443−3457.

(13) Deloach, L. D.; Payne, S. A.; Chase, L. L.; Smith, L. K.; Kway, W. L.; Krupke, W. F. Evaluation of Absorption and Emission Properties of Yb³⁺ Doped Crystals for Laser Applications. *IEEE J. Quantum Electron.* **1993**, *29* (4), 1179−1191.

(14) Schmidt, J.; Penzkofer, A. Absorption Cross-Sections, Saturated Vapor-Pressures, Sublimation Energies, and Evaporation Energies of Some Organic Laser-Dye Vapors. *J. Chem. Phys.* **1989**, *91* (3), 1403−1409.

(15) Zou, W. Q.; Visser, C.; Maduro, J. A.; Pshenichnikov, M. S.; Hummelen, J. C. Broadband dye-sensitized upconversion of near-infrared light. *Nat. Photonics* **2012**, *6* (8), 560−564.

(16) Chen, G. Y.; Agren, H.; Ohulchanskyy, T. Y.; Prasad, P. N. Light upconverting core-shell nanostructures: nanophotonic control for emerging applications. *Chem. Soc. Rev.* **2015**, *44* (6), 1680−1713.

(17) Singh-Rachford, T. N.; Castellano, F. N. Photon upconversion based on sensitized triplet-triplet annihilation. *Coord. Chem. Rev.* **2010**, *254* (21−22), 2560−2573.

(18) Zhou, J.; Liu, Q.; Feng, W.; Sun, Y.; Li, F. Y. Upconversion Luminescent Materials: Advances and Applications. *Chem. Rev.* **2015**, *115* (1), 395−465.

(19) Chen, G. Y.; Ohulchanskyy, T. Y.; Kumar, R.; Agren, H.; Prasad, P. N. Ultrasmall Monodisperse NaYF₄:Yb³⁺/Tm³⁺ Nanocrystals with Enhanced Near-Infrared to Near-Infrared Upconversion Photoluminescence. *ACS Nano* **2010**, *4* (6), 3163−3168.

(20) Wang, G. F.; Qin, W. P.; Wang, L. L.; Wei, G. D.; Zhu, P. F.; Kim, R. J. Intense ultraviolet upconversion luminescence from hexagonal NaYF₄: Yb³⁺/Tm³⁺ microcrystals. *Opt. Express* **2008**, *16* (16), 11907−11914.

(21) Clapp, A. R.; Medintz, I. L.; Mauro, J. M.; Fisher, B. R.; Bawendi, M. G.; Mattoussi, H. Fluorescence resonance energy transfer between quantum dot donors and dye-labeled protein acceptors. *J. Am. Chem. Soc.* **2004**, *126* (1), 301−310.

(22) Bednarkiewicz, A.; Wawrzynczyk, D.; Nyk, M.; Strek, W. Synthesis and spectral properties of colloidal Nd³⁺ doped NaYF₄ nanocrystals. *Opt. Mater.* **2011**, *33* (10), 1481−1486.

(23) Xu, C. T.; Svenmarker, P.; Liu, H. C.; Wu, X.; Messing, M. E.; Wallenberg, L. R.; Andersson-Engels, S. High-Resolution Fluorescence Diffuse Optical Tomography Developed with Nonlinear Upconverting Nanoparticles. *ACS Nano* **2012**, *6* (6), 4788−4795.

(24) Xie, X. J.; Gao, N. Y.; Deng, R. R.; Sun, Q.; Xu, Q. H.; Liu, X. G. Mechanistic Investigation of Photon Upconversion in Nd³⁺-Sensitized Core-Shell Nanoparticles. *J. Am. Chem. Soc.* **2013**, *135* (34), 12608−12611.

(25) Wang, Y. F.; Liu, G. Y.; Sun, L. D.; Xiao, J. W.; Zhou, J. C.; Yan, C. H. Nd³⁺-Sensitized Upconversion Nanophosphors: Efficient In Vivo Bioimaging Probes with Minimized Heating Effect. *ACS Nano* **2013**, *7* (8), 7200−7206.

(26) Zhong, Y. T.; Tian, G.; Gu, Z. J.; Yang, Y. J.; Gu, L.; Zhao, Y. L.; Ma, Y.; Yao, J. N. Elimination of Photon Quenching by a Transition Layer to Fabricate a Quenching-Shield Sandwich Structure for 800 nm Excited Upconversion Luminescence of Nd³⁺ Sensitized Nanoparticles. *Adv. Mater.* **2014**, *26* (18), 2831−2837.

(27) Dong, A. G.; Ye, X. C.; Chen, J.; Kang, Y. J.; Gordon, T.; Kikkawa, J. M.; Murray, C. B. A Generalized Ligand-Exchange Strategy Enabling Sequential Surface Functionalization of Colloidal Nanocrystals. *J. Am. Chem. Soc.* **2011**, *133* (4), 998−1006.

(28) Suyver, J. F.; Aebischer, A.; Garcia-Revilla, S.; Gerner, P.; Gudel, H. U. Anomalous power dependence of sensitized upconversion luminescence. *Phys. Rev. B: Condens. Matter Mater. Phys.* **2005**, *71* (12), 125123 DOI: 10.1103/PhysRevB.71.125123.

(29) Ward, M. D. Mechanisms of sensitization of lanthanide(III)-based luminescence in transition metal/lanthanide and anthracene/lanthanide dyads. *Coord. Chem. Rev.* **2010**, *254* (21−22), 2634−2642.

(30) Kim, J. H.; Deng, F.; Castellano, F. N.; Kim, J. H. High Efficiency Low-Power Upconverting Soft Materials. *Chem. Mater.* **2012**, *24* (12), 2250−2252.